

Laser-bandwidth-induced fluctuations in the intensity transmitted by a Fabry-Pérot interferometer

G. Klimeck and D. S. Elliott

School of Electrical Engineering, Purdue University, West Lafayette, Indiana 47907

M. W. Hamilton

Department of Physics and Applied Physics, University of Strathclyde, Glasgow, G4 0NG Scotland

(Received 4 March 1991)

We have measured the power spectrum of the intensity fluctuations of light transmitted by a Fabry-Pérot interferometer when the input field is the real Gaussian field. The real Gaussian field is a field characterized by real, random (Gaussian) amplitude fluctuations. The bandwidth of the real Gaussian field was varied, taking on values less than that of the interferometer, as well as greater. Comparisons of the measured spectra with calculated spectra are quite satisfactory. Of special interest is a feature in the spectra centered at the laser-interferometer detuning frequency.

INTRODUCTION

Laser-bandwidth effects on nonlinear-optical processes have been of growing interest for the past two decades, but recently systems that are inherently linear in their response to the electromagnetic wave have shown interesting laser-bandwidth effects as well. These linear systems become interesting when higher-order correlation properties of the system are involved. An example of this is the fluctuations (rather than just the average value) of fluorescence from a linear atomic system interacting with weak laser radiation. Observations [1,2] of an unusual dependence of fluorescence fluctuations on laser detuning from resonance with the atoms motivated several theoretical works [3-5]. Recent measurements of the variance [6] and of the spectrum [7] of these fluctuations when the atom is excited by a phase diffusing laser field are in good agreement with theory. In this paper, we discuss measurements of the spectrum of fluctuations of laser light transmitted by a Fabry-Pérot interferometer when the input field undergoes random amplitude fluctuations. The field is described by the model known as the real Gaussian field. The Fabry-Pérot interferometer is a linear system for all intensities used in this work, and measurements are in excellent agreement with calculations [8].

EXPERIMENTAL TECHNIQUE

Generation of the real Gaussian field has been discussed in detail in a previous publication [9]. The field is of the form

$$E(t) = \varepsilon(t)e^{i\omega_L t}, \quad (1)$$

where ω_L is a constant frequency. The amplitude $\varepsilon(t)$ is a Gaussian random process with an average value of zero; i.e., it is positive as often as it is negative. This field is generated by modulating the output of highly stabilized cw tunable dye laser using an acousto-optic modulator (AOM). The AOM is driven by a rf signal whose ampli-

tude is also a real Gaussian process. Laser bandwidths from 1 to 14 MHz full width at half maximum (FWHM) are attainable. The lower limit is determined by the bandwidth of the stabilized dye laser (~ 200 kHz). Measurements of the power spectrum of the intensity fluctuations of the real Gaussian field intensity indicate that it falls off with frequency slightly faster than a Lorentzian. For all laser bandwidths used in this experiment, the measured intensity spectrum is about 3 dB below a real Lorentzian at about 25 MHz, and about 7.5 dB lower at 40 MHz. Three factors contribute to this sub-Lorentzian shape. First is the response of the AOM. The efficiency of the AOM is at a maximum for a drive frequency of 200 MHz, and falls off by about 3 dB when the drive signal is 50 MHz to either side of 200 MHz. Second is the spatial coherence of the beam diffracted by the AOM. When the AOM drive signal is modulated, the acoustic wave in the modulator is not uniform across the optical wave front. This leads to a variation of the amplitude of the real Gaussian field across the beam. Since the intensity spectrum is measured by projecting the entire beam onto a photodiode, the average intensity is measured, so that the higher-frequency components of the fluctuations tend to average out. Both of these processes are discussed in more detail in Ref. [9]. An additional contribution to the decrease in the high-frequency components is the frequency response of the detector itself. This is secondary to the preceding two effects. Approximately 4% of the incident field intensity can be converted into the real Gaussian field. Higher diffraction efficiencies or larger bandwidths result in distortion of the signal, such that $\varepsilon(t)$ deviates from a Gaussian process. This limit was determined through measurements of the intensity autocorrelation function, which for the perfect real Gaussian field with a Lorentzian power spectrum decreases exponentially from an initial value of three to a long-term value of 1:

$$R_I(\tau) = \frac{\langle I(t+\tau)I(t) \rangle}{\langle I(t) \rangle^2} = 1 + 2e^{-2b|\tau|}, \quad (2)$$

where $2b$ is the width (FWHM) of the Lorentzian laser line in angular frequency. In practice, initial values of $R_I(0)$ are measured to be in the range 2.4–2.8. Figure 1 shows a typical measurement of the intensity of the real Gaussian field and the corresponding intensity autocorrelation function computed from a series of these digitized traces.

The Fabry-Pérot interferometer is of near confocal geometry with a free spectral range (FSR) of 4 GHz. The interferometer is a commercial model of an optical scanning spectrum analyzer, from which we have removed the photodiode detector and modified the mechanism for adjusting the cavity length. The rear mirror of the interferometer is mounted on a shaft whose position is adjusted using a 40 pitch screw, and locked in place by tighten-

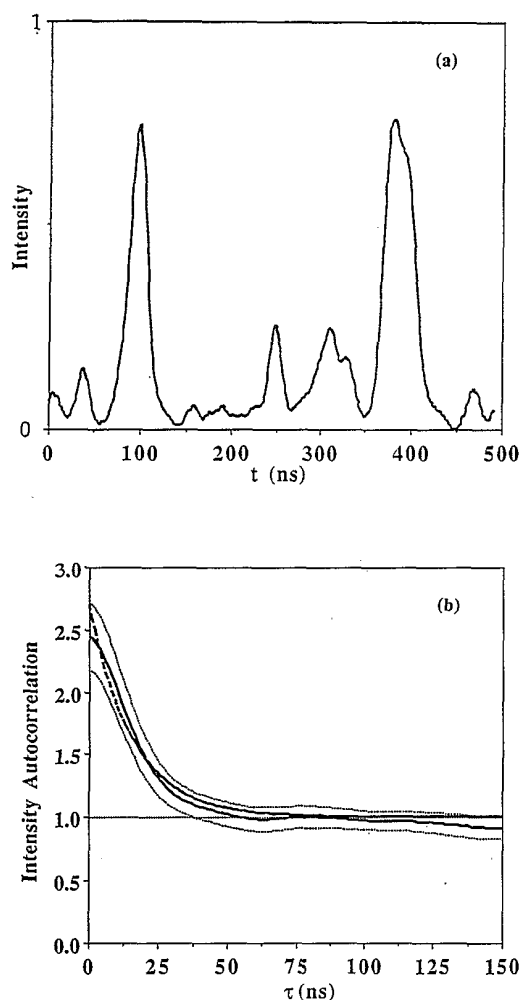


FIG. 1. (a) Typical time trace of the intensity of the real Gaussian field, and (b) the intensity autocorrelation function computed from 26 such traces. The bandwidth of the laser was $b/\pi = 9.0$ MHz (FWHM) for this figure, leading to a correlation time of the intensity fluctuations of $1/2b = 18$ nsec. In (b) the measured autocorrelation (solid line) is shown, as well as the result of a least-squares fitting procedure to a function of the form $1 + [R_I(0) - 1]\exp(-2b\tau)$ (dashed curve). The dotted curves indicate the standard deviation of the measured autocorrelation function, as determined from the scatter of the data.

ing a collet nut. This allows fine tuning of the cavity length to within approximately $10 \mu\text{m}$ of confocal geometry, as evidenced by measurements of the cavity transmission peak width, to be discussed later.

Mode matching of the Gaussian laser beam into the confocal cavity was important in order to make interpretation of the results simpler. Calculations [8] of the bandwidth effects were carried out for excitation of a single transverse and longitudinal mode of the cavity. The laser beam was focused to the center of the cavity using an $f = 22$ -cm focal length achromatic doublet. The e^{-2} beam radius before focusing was 0.61 mm. The coupling [10] into the TEM_{nm} ($n + m$ even) modes was nearly perfect, as confirmed by observing the mode pattern of the transmitted beam visually, and by measurements of the intensity of the various transverse modes as the interferometer was scanned. We estimate that while the $\text{TEM}_{0,0}$ cavity mode dominates, a few other higher-order even modes were also excited, as observed by slight misadjustment of the cavity from confocal separation. A cavity length differing from that of a confocal geometry by as little as $15 \mu\text{m}$, for example, would result in a shift between the even-order modes of about 1 MHz. This causes the transmission peak to become asymmetric and somewhat broader when higher-order even modes are also excited. Our previous claim of the precision of the adjustment of the cavity length is based on the high degree of symmetry we observed. The peak height corresponding to the odd values of $n + m$ was reduced to less than $\frac{1}{50}$ the peak height of the even modes. Overall mode matching was, we believe, quite satisfactory, although the effect of a mismatch is not well understood.

In order to measure bandwidth effects, it was necessary to control the detuning of the laser frequency from resonance with the cavity. This was accomplished using standard frequency locking techniques, as shown in Fig. 2. The output of the dye laser was split into two parts, one of which was modulated to produce the real Gaussian field, while the second was used for locking the laser frequency to the cavity. We will refer to these beams as the Gaussian and locking beams, respectively. The center frequency of the real Gaussian field was shifted by the AOM by $\nu_G = 200$ MHz. The locking beam was frequency shifted by a second AOM which was driven by a single-tone frequency modulated signal. The carrier of this drive signal was varied in frequency ν_1 from 160 to 240 MHz, and was frequency modulated at 10 kHz. The deviation frequency of the modulation was about 8 MHz. The polarization of the locking beam was rotated 90° , and the Gaussian and locking beams were recombined on a polarizing beamsplitter. The two beams passed through the interferometer collinearly, and were separated with a second polarizing beamsplitting cube upon exiting the interferometer. Cross coupling between the two beams was observed to be negligible. An error signal was generated from the locking beam photocurrent by demodulation of the 10 -kHz dither in a lock-in amplifier. The lock-in output was integrated, amplified and applied to the frequency tune control of the dye laser, thus keeping the locking beam resonant with the interferometer. Since the Gaussian and locking beams differed in frequency by

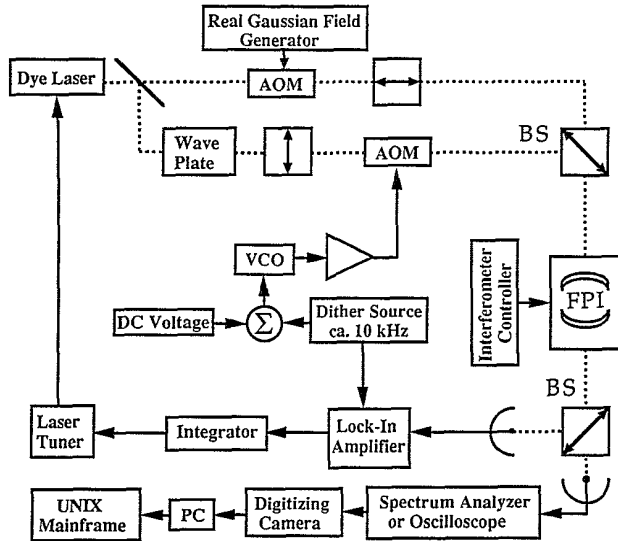


FIG. 2. Schematic diagram of the experiment. The output of the tunable dye laser is split into two beams, one which is randomly amplitude modulated to form the real Gaussian field, the other of which is single-tone frequency modulated to lock the laser frequency to the peak of the interferometer transmission peak. The two beams pass through the interferometer (FPI) collinearly, and are separated using a polarizing beam splitter cube (BS). The locking beam is detected, amplified in a lock-in detector, and integrated to produce a feedback signal to correct the frequency of the dye laser. The real Gaussian field intensity is spectrally analyzed, digitized, and stored on a personal computer (PC).

$\Delta = \nu_G - \nu_1$, the detuning of the Gaussian beam from cavity resonance was also Δ . This scheme was used for measurement of the cavity finesse as well as for measurements of laser bandwidth effects.

For the finesse measurements, the noise modulation electronics were replaced by a single frequency source so that the "Gaussian" beam was narrow band, and the average transmitted intensity was recorded as a function of Δ . These data are shown on a logarithmic scale in Fig. 3. The circles represent the data points and the solid line represents the result of a least-squares fit of a Lorentzian curve to the data, yielding a bandwidth (FWHM) of about 11.5 MHz. This corresponds to a cavity finesse of 350. The data and the fit agree very nicely for detunings Δ greater than -10 MHz. For larger negative detunings, the poor agreement is due, we believe, to misalignment of the locking beam from the axis of the interferometer. In support of this assertion, we note that the hump on the low-frequency side of this curve is not evident when simply scanning the interferometer with the laser frequency fixed. Misalignment results from changing the carrier frequency of the locking beam, since the diffraction angle in the AOM varies with the drive frequency. For drive frequencies less than 190 MHz (detunings less than -10

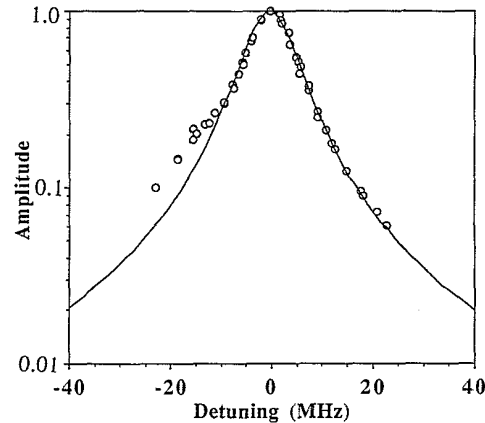


FIG. 3. The average intensity transmitted by the Fabry-Pérot interferometer. The open circles represent the measured intensities, while the curve represents a fit to the data of a Lorentzian function. From these data, the width of the transmission peak is determined to be 11.5 MHz, corresponding to a finesse of 350.

MHz), it appears that the locking laser excites a different mode of the cavity sufficiently to cause the system to lock to the peak of that mode. This shifts the detuning of the Gaussian beam, such that detuning measurements below -10 MHz are not accurate. We therefore limited our measurements to detunings outside this range.

The measurements of the power spectrum of the intensity noise transmitted by the interferometer are carried out by projecting the transmitted Gaussian beam onto a silicon photodiode, whose photocurrent is measured on a rf spectrum analyzer. The spectra are measured in the range of frequencies from 3 to 39 MHz, for detunings of the Gaussian laser from resonance of 0–35 MHz. The laser bandwidth was adjusted to 4.8, 9.0, or 14.0 MHz (FWHM). Up to 23 power spectra of the intensity fluctuations were measured in each data set, and two data sets were recorded for each value of laser bandwidth. The intensity autocorrelation was checked for each laser bandwidth as well, yielding initial values of $R_I(0) = 2.55$, 2.57, and 2.44, respectively. Results will be presented in the following section, where we show very good agreement with calculated results.

RESULTS

A few examples of the power spectra of the intensity fluctuations transmitted by the Fabry-Pérot interferometer are shown in Fig. 4. Figures 4(a), 4(b), and 4(c) correspond to laser bandwidths of 4.8, 9.0, and 14.0 MHz, respectively. For each diagram spectra are shown for laser-resonator detunings Δ of 0, 10, 20, and 30 MHz, from top to bottom. Each diagram shows the measured spectra (rough lines) as well as the calculated spectra (smooth lines). We will first discuss the calculated curves, which are of the form

$$S_I(\omega) = \sum_{i=1,2} A \left[\frac{4b}{\omega^2 + (2b)^2} + \frac{2 \operatorname{Re}(B_i)(b + \Delta\omega_c) + 2 \operatorname{Im}(B_i)(\Delta + \omega)}{(\Delta + \omega)^2 + (b + \Delta\omega_c)^2} + \frac{2 \operatorname{Re}(B_i)(b + \Delta\omega_c) + 2 \operatorname{Im}(B_i)(\Delta - \omega)}{(\Delta - \omega)^2 + (b + \Delta\omega_c)^2} + \frac{|B_i|^2 4\Delta\omega_c}{\omega^2 + (2\Delta\omega_c)^2} \right], \quad (3)$$

where $\Delta\omega_c$ is the cavity width half width at half maximum, equal in our case to $\pi(11.5)$ MHz, and

$$\begin{aligned} A &= |(1 - \operatorname{Re} e^{b\tau' + i\delta})(1 - \operatorname{Re} e^{-b\tau' - i\delta})|^{-2}, \\ B_1 &= \frac{\operatorname{Re} e^{i\delta}(e^{-b\tau'} - e^{b\tau'})}{1 - R^2} \frac{1 - \operatorname{Re} e^{-b\tau' - i\delta}}{1 - \operatorname{Re} e^{-b\tau' + i\delta}}, \\ B_2 &= \frac{\operatorname{Re} e^{i\delta}(e^{-b\tau'} - e^{b\tau'})}{1 - R^2 e^{2i\delta}}. \end{aligned} \quad (4)$$

Note that although the B 's are complex, the power spectrum is always real and positive, as required. R is the reflectance of the interferometer mirrors, and is related to the cavity width by $\Delta\omega_c = -(1/\tau') \ln R$, where τ' is the cavity round-trip time. δ is the cavity round trip phase shift, equal to $\omega_L \tau'$. Equation (3) shows that there are several contributions to the power spectrum of the intensity fluctuations of the transmitted radiation. We can understand these terms qualitatively by considering a simple

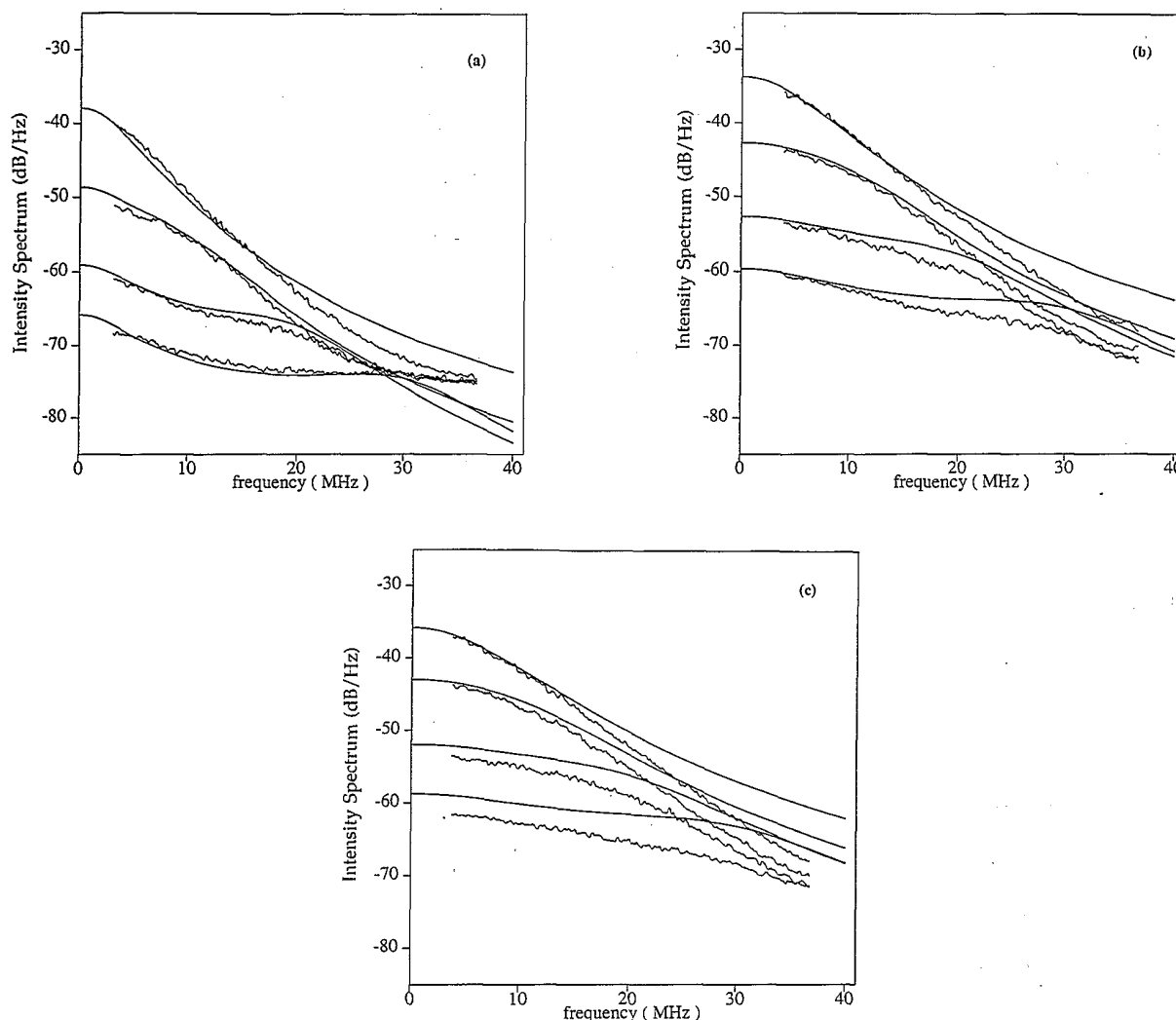


FIG. 4. Power spectra of the intensity fluctuations of the transmitted light. The laser bandwidth (FWHM) in the figure are (a) 4.8 MHz, (b) 9.0 MHz, and (c) 14.0 MHz. The width of the interferometer peak is 11.5 MHz. In each figure the data (rough curves) and calculations (smooth curves) are shown. The four sets of curves in each figure correspond to a laser-interferometer detuning Δ of 0, 10, 20, and 30 MHz, from top to bottom.

picture of the transmitted field. The transmitted-field spectrum should be expected to exhibit two maxima, one at the laser frequency, the other at the cavity resonant frequency. The intensity spectrum, therefore, consists of peaks with maxima at zero frequency corresponding to each of these peaks beating against themselves, and also a peak centered at the detuning frequency resulting from the two peaks of the field spectrum beating against each other. These are illustrated in Fig. 5, where we have plotted each term in Eq. (3) for a laser of width 9.0 MHz, a cavity of width 11.5 MHz, and a detuning frequency of 30 MHz. The first and last terms in Eq. (3) are Lorentzian in shape, and have widths equal to twice the laser width and twice the cavity width, respectively. These terms correspond to curves *b* and *c* in Fig. 5. The Lorentzian curve (*d*) and dispersion-shaped curve (*e*) centered at 30 MHz in Fig. 5 are represented in Eq. (3) by the terms involving $\text{Re}(B_i)$ and $\text{Im}(B_i)$, respectively. These terms represent the cross term between the two peaks in the transmitted-field spectrum. The dispersion-shaped curve was omitted from the results in Ref. [8], due to an error made in evaluating the Fourier transform of Eq. (27) and (28) of that work. We also remark here that Eq. (27) and (28) of Ref. [8], while they are not incorrect, could have been represented in a much simpler form. See the Appendix for further discussion.

Several features of the measured data are noteworthy. The overall shape of the data curves are in very good agreement with the calculated curves. Within each figure, the only adjustment made to the calculated curves is an overall amplification, which on a logarithmic scale of course corresponds to a vertical displacement. The relative amplitudes of each of the curves within any of the figures are not adjusted. The data curves tend to fall off

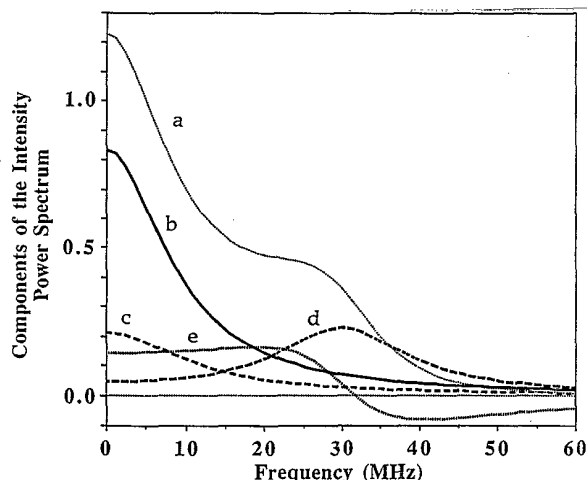


FIG. 5. Components of the calculated spectrum of the intensity fluctuations. The laser width for these curves is 4.5 MHz, the interferometer width is 11.5 MHz, and the detuning Δ is 30 MHz. The five curves in the figure represent the various terms of Eq. (3) in the text. They are (a) the total power spectrum, (b) the laser bandwidth Lorentzian, (c) the cavity bandwidth Lorentzian, (d) the Lorentzian cross term, and (e) the dispersion-shaped cross term.

with frequency slightly faster than the calculated results, which we attribute to the spatial averaging and the frequency response of the detection system. Figure 6 shows the frequency response of the random-modulation system. This was measured by single-tone modulating the field amplitude at a frequency ν_m , suppressing the carrier, removing the interferometer, and measuring the amplitude of the current generated by the photodiode at the frequency $2\nu_m$. Using the frequency response shown in Fig. 6 to adjust our data actually overcompensates at high frequencies. That this correction does not apply perfectly is not surprising since no account is taken of the effect of the Fabry-Pérot interferometer on the transmission of a field with imperfect spatial coherence. The spatial coherence of the real Gaussian field was discussed earlier in the context of the laser intensity band shape. Nevertheless, the correction factor is of the proper order to explain the difference between the data and calculated curves. The data for a laser width of 4.8 MHz shows at higher frequencies a contribution from the noise level of the spectrum analyzer.

In Fig. 7 we show the amplitude of the power spectrum at zero frequency versus detuning for the data. The curves represent the calculated amplitudes. Each curve and data set has been normalized to a peak value of 1. The data points are obtained by extrapolating the measured power spectra to zero frequency. Agreement is good for all laser bandwidths used, with the exception of the 14.0-MHz data for detuning frequencies greater than 20 MHz. In this range the amplitude of the fluctuations is measured to be less than that calculated, probably due to the sub-Lorentzian power spectrum of the laser for high frequencies.

We have found poor agreement when comparing measured and calculated bandwidths of the intensity spectra. This is not surprising, however, when one considers the limited frequency response of the measurements due to spatial coherence of the field and the detection system.

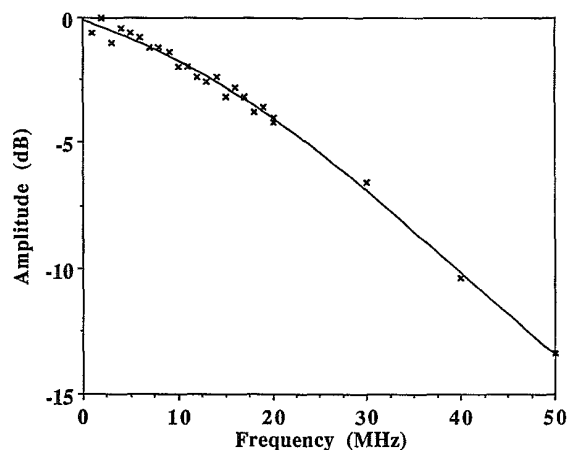


FIG. 6. Frequency response of the system: The measured amplitude of the sidebands of the laser when single-tone amplitude modulated with a suppressed carrier.

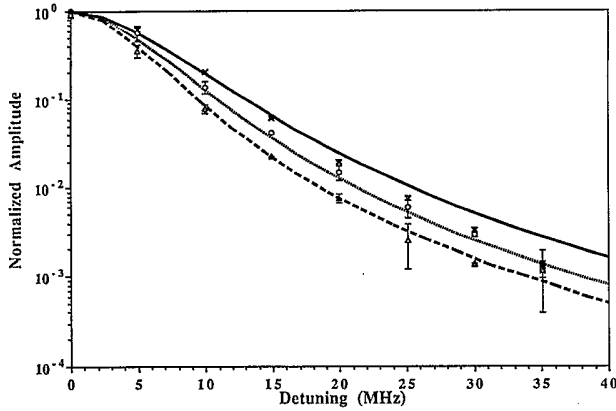


FIG. 7. Normalized amplitude of the intensity power spectra at zero frequency as a function of the laser-interferometer detuning Δ . The points correspond to measurement for laser widths of 4.8 MHz (\triangle), 9.0 MHz (\circ), and 14.0 MHz (\times), while the curves are derived from calculated power spectra, for the same laser bandwidth values (dashed, dotted, and solid lines, respectively).

In conclusion, we have presented results of measurements of the power spectrum of the intensity fluctuations of light transmitted by a Fabry-Pérot interferometer when a real Gaussian field is incident upon it. Agreement of the measured spectra with those calculated previously is very good, particularly when examining relative amplitudes, the cross term “hump” at the detuning frequency, and the overall shape of the curves. These measurements display very nicely the effect of a linear system, the interferometer, on the higher-order statistical properties of the field.

ACKNOWLEDGMENTS

This work was supported by a grant from the U.S. Department of Energy, Office of Basic Energy Sciences. Participation by M.W.H. was made possible by a Collaborative Research Grant from the NATO Scientific Affairs Division. One of us (G.K.) is grateful to the Friedrich-Ebert Stiftung for their financial support. We would like to thank Bruce Ferguson for many useful discussions during the course of this work.

APPENDIX

In this appendix we discuss a simplification of the derivation and the results of Ref. [8] for the intensity correlation function of the field transmitted by a Fabry-Pérot interferometer when a thermal field or a real Gaussian field is incident upon it. Each field is represented by Eq. (1), where $\epsilon(t)$ is a real Gaussian variable for the real Gaussian field, and a complex variable for the thermal field. In the latter case we represent $\epsilon(t)$ as $\epsilon'(t) + i\epsilon''(t)$, where $\epsilon'(t)$ and $\epsilon''(t)$ are each real Gaussian processes, independent of each other but of the same spectral density. After being transmitted by the interferometer, the spectral density of $\epsilon(t)$ is modified, but

since the filter is linear, the amplitude is still a Gaussian variable. Preservation of the Gaussian properties is necessary for a subsequent step. The intensity correlation function $R_I^0(\tau)$ of the transmitted field is given by

$$R_I^0(\tau) = \frac{\langle I_0(t+\tau)I_0(t) \rangle}{\langle I(t) \rangle^2} = \frac{\langle |E_0(t+\tau)|^2 |E_0(t)|^2 \rangle}{\langle |E(t)|^2 \rangle^2}. \quad (\text{A1})$$

The “0” denotes the transmitted field or intensity. We normalize to the average input intensity in order to retain information on the magnitude of the fluctuations. In order to evaluate this autocorrelation function for the output intensity fluctuations, we need to relate the transmitted field to the incident field. This is done in the usual series expansion

$$E_0(t) = \epsilon_0(t) e^{i\omega_L t} = (1 - R) [\epsilon(t) + R\epsilon(t - \tau') e^{-i\delta} + R^2 \epsilon(t - 2\tau') e^{-2i\delta} + \dots] e^{i\omega_L t}, \quad (\text{A2})$$

where each term represents one more round-trip of the field through the cavity than the previous term. We then write the intensity correlation function in terms of the transmitted-field amplitude

$$R_I^0(\tau) = \langle \epsilon_0(t+\tau) \epsilon_0^*(t+\tau) \epsilon_0(t) \epsilon_0^*(t) \rangle / \langle |\epsilon(t)|^2 \rangle^2. \quad (\text{A3})$$

Since the amplitude of the transmitted field $\epsilon_0(t)$ is a Gaussian variable, this fourth-order correlation function can be decomposed into a sum of products of second-order correlation functions,

$$R_I^0(\tau) = [\langle |\epsilon_0(t)|^2 \rangle^2 + \langle \epsilon_0(t+\tau) \epsilon_0(t) \rangle^2 + \langle \epsilon_0^*(t+\tau) \epsilon_0(t) \rangle^2] / \langle |\epsilon(t)|^2 \rangle^2. \quad (\text{A4})$$

The first term here is the square of the average transmitted intensity. The second term vanishes for the thermal field since $\epsilon(t)$ is complex and of random phase. Therefore, when the thermal field is incident on the interferometer, the autocorrelation function is

$$R_{I,\text{th}}^0(\tau) = \langle I \rangle^2 + \langle \epsilon_0^*(t+\tau) \epsilon_0(t) \rangle^2 / \langle |\epsilon(t)|^2 \rangle, \quad (\text{A5})$$

and when the real Gaussian field is incident,

$$R_{I,\text{RGF}}^0(\tau) = R_{I,\text{th}}^0(\tau) + \langle \epsilon_0(t+\tau) \epsilon_0(t) \rangle^2 / \langle |\epsilon(t)|^2 \rangle. \quad (\text{A6})$$

Equation (A4) represents a significant simplification over the procedure outlined in Ref. [8]. Each of the second-order correlation functions in (A4) involve a product of two infinite summations of the field given by (A2). This summation can be simplified by regrouping terms according to their order in R , and the input field amplitude correlation functions evaluated using $\langle \epsilon^*(t+\tau) \epsilon(t) \rangle /$

$|\varepsilon(t)|^2 = e^{-\beta|t|}$. After contracting the resulting summations we find the following expressions:

$$\frac{\langle \varepsilon_0^*(t+\tau)\varepsilon_0(t) \rangle}{\langle |\varepsilon(t)|^2 \rangle} = (1-R)^2 \left[\frac{e^{-b\tau}}{(1-\text{Re}^{b\tau'+i\delta})(1-\text{Re}^{-b\tau'-i\delta})} + \frac{(\text{Re}^{-b\tau'+i\delta})^{M+1}e^{b\tau}}{(1-\text{Re}^{-b\tau'-i\delta})(1-R^2e^{-2i\delta})} + \frac{(\text{Re}^{b\tau'+i\delta})^{M+1}e^{-b\tau}}{(1-\text{Re}^{b\tau'-i\delta})(1-R^2e^{-2i\delta})} \right] \quad (\text{A8})$$

$$= (1-R)^2 \left[\frac{e^{-b\tau}}{(1-\text{Re}^{b\tau'+i\delta})(1-\text{Re}^{-b\tau'-i\delta})} + \frac{(\text{Re}^{-b\tau'+i\delta})^{M+1}e^{b\tau}}{(1-\text{Re}^{-b\tau'-i\delta})(1-R^2)} - \frac{(\text{Re}^{b\tau'+i\delta})^{M+1}e^{-b\tau}}{(1-\text{Re}^{b\tau'-i\delta})(1-R^2)} \right] \quad (\text{A7})$$

and

M in these expressions is the integer value of τ/τ' . In the usual case of bandwidths much smaller than the FSR of the cavity, M can be substituted by τ/τ' , leading to the power spectrum in the text, Eq. (3).

-
- [1] C. Weiman and C. Tanner (private communication). 1346 (1990).
 [2] L. Hollberg (private communication). [7] M. H. Anderson, R. D. Jones, J. Cooper, S. J. Smith, D. S. Elliott, H. Ritsch, and P. Zoller, Phys. Rev. A **42**, 6690 (1990).
 [3] Th. Haslwanter, H. Ritsch, J. Cooper, and P. Zoller, Phys. Rev. A **38**, 5652 (1988). [8] B. A. Ferguson and D. S. Elliott, Phys. Rev. A **41**, 6183 (1990).
 [4] K. Rzazewski, B. Stone, and M. Wilkens, Phys. Rev. A **40**, 2788 (1989). [9] Cheng Xie, G. Klimeck, and D. S. Elliott, Phys. Rev. A **41**, 6376 (1990).
 [5] H. Ritsch, P. Zoller, and J. Cooper, Phys. Rev. A **41**, 2653 (1990). [10] J. T. Verdeyen, *Laser Electronics*, 2nd ed. (Prentice Hall, Englewood Cliffs, NJ, 1989), pp. 134 and 135.
 [6] M. H. Anderson, R. D. Jones, J. Cooper, S. J. Smith, D. S. Elliott, H. Ritsch, and P. Zoller, Phys. Rev. Lett. **64**,